Journal of Biomolecular NMR, 4 (1994) 553–574
ESCOM

J-Bio NMR 191

^{1}H, ^{15}N, ^{13}C and ^{13}CO resonance assignments and secondary structure of villin 14T, a domain conserved among actin-severing proteins

Michelle A. Markus[a,b], Tomoko Nakayama[c], Paul Matsudaira[c] and Gerhard Wagner[a,b,*]

[a]*Committee on Higher Degrees in Biophysics, Harvard University, Cambridge, MA 02138, U.S.A.*
[b]*Department of Biological Chemistry and Molecular Pharmacology, Harvard Medical School, 240 Longwood Avenue, Boston, MA 02115, U.S.A.*
[c]*Whitehead Institute for Biomedical Research, Nine Cambridge Center and Department of Biology, Massachusetts Institute of Technology, Cambridge, MA 02142, U.S.A.*

Received 28 December 1993
Accepted 1 February 1994

Keywords: Villin 14T; Heteronuclear multidimensional NMR; Chemical shift assignments; Hydrogen exchange; Calcium titration; pH titration

SUMMARY

Sequence-specific assignments have been made for the ^{1}H, ^{15}N, ^{13}C and ^{13}CO resonances of 14T, the 126-residue amino-terminal domain of the actin-severing protein villin. Villin is a member of a family of proteins that regulate cytoskeletal actin by severing, capping and nucleating actin filaments. Actin binding is dependent on calcium and disrupted by phosphatidyl inositol 4,5-bisphosphate. Actin-severing proteins are built from three or six repeats of a conserved domain, represented by 14T. Expression in *Escherichia coli* facilitated incorporation of ^{15}N and ^{13}C isotopes and application of triple-resonance, backbone-directed strategies for the sequential assignments. Elements of regular secondary structure have been identified by characteristic patterns of NOE cross peaks and values of vicinal $^{3}J_{H^N H^\alpha}$ coupling constants. Amide protons that exchange slowly (rates less than 1.0×10^{-4} per min) are concentrated in the central β-sheet and the second and third α-helices, suggesting that these elements of secondary structure form very stable hydrogen bonds. Assignments for the amide nitrogens and protons have been examined as a function of pH and calcium concentration. Based on the conservation of chemical shifts in the core of the domain, villin 14T maintains the same overall fold in the pH range from 4.15 to 6.91 and the calcium range from 0 to 50 mM. The calcium data indicate the presence of two calcium-binding sites and suggest their locations.

INTRODUCTION

Actin-severing proteins influence the framework of eukaryotic cells by regulating cytoskeletal actin filaments (Matsudaira and Janmey, 1988). In the presence of Ca^{2+} cations, these proteins

*To whom correspondence should be addressed.

sever and cap actin filaments. Addition of phosphatidyl inositol 4,5-bisphosphate releases the caps to allow filament elongation (Janmey and Matsudaira, 1988). Actin-severing proteins can also recruit actin monomers to nucleate filament growth. Sequence analysis and limited proteolysis have revealed that actin-severing proteins are built from three or six repeats of an approximately 130-residue domain (Bazari et al., 1988; Way and Weeds, 1988). The isolated amino-terminal domains from two members of this family, gelsolin and villin, show Ca^{2+}-dependent actin-monomer binding (Janmey and Matsudaira, 1988). This suggests that the functions of the actin-severing proteins result from interaction between multiple actin-binding sites within the proteins and various forms of actin (Pope et al., 1991; Way et al., 1992).

Although the actin-severing proteins are built from repeats of a fundamental domain, the behavior of this domain differs depending on the context. For example, though the domain structure implies six actin-binding sites, biochemical studies identify only three – a monomer-binding site in the first domain, a filament-binding site in domains two and three, and another monomer-binding site in domains four through six (Pope et al., 1991). As another example, despite 45% sequence identity, villin requires higher Ca^{2+} concentrations for activity than gelsolin (Janmey and Matsudaira, 1988). Villin is unique among the actin-severing proteins in that it also bundles actin filaments in the context of absorptive epithelial cells to form microvilli. Thus, its requirement for high levels of Ca^{2+} may reflect an adaptation to prevent severing while bundling filaments. A detailed understanding of the mechanisms of interaction with actin must include molecular-level explanations for these differences.

We have undertaken assignments of the amino-terminal domain of villin, 14T, as a first step toward structural studies of the domain in solution. These assignments have already led to a preliminary structure of the free domain (Markus et al., 1994). The general form of the domain bears a striking resemblance to the actin-binding protein profilin (Archer et al., 1993; Metzler et al., 1993; Schutt et al., 1993; Vinson et al., 1993). A detailed look at the sequences and topology shows that profilin and villin use residues from different sequential positions to fold into a similar overall shape. The fold of 14T more closely resembles that of the amino-terminal domain of gelsolin, whose structure has been solved by X-ray crystallography in a complex with actin (McLaughlin et al., 1993). With the assignments for 14T, we can use chemical shifts as an atomic-resolution probe into the solution structure. Focusing on the chemical shifts for the amide nitrogens and protons, we have studied the structure at different pH values and calcium concentrations. A more complete description of the mechanisms of activity for actin-severing proteins will result from further studies of villin in solution, based on the assignments reported here.

MATERIALS AND METHODS

Sample preparation

Details of expression and purification will be presented elsewhere (Nakayama, T., Way, M., Weeds, A. and Matsudaira, P., manuscript in preparation). Briefly, residues 1–126 of the chicken epithelial villin sequence were expressed in *Escherichia coli* (strain BL21(DE3)) with the T7-based pAED4 vector (de Arruda et al., 1992). Cells were induced with IPTG and grown for several hours before harvest and lysis by sonication. Lysate was clarified by centrifugation and passed over a DEAE Sepharose (Pharmacia) column. The DEAE flow-through was dialyzed into succinate at pH 5.5 and loaded onto a carboxymethyl Sepharose (Pharmacia) column. Villin 14T

adsorbed and was eluted with a gradient in NaCl. The main eluted peak corresponds to 14T and was judged more than 95% pure by SDS-PAGE. For unlabeled protein, cells were grown in rich medium. For isotope-labeled protein, cells were grown in M9 minimal medium with ^{13}C glucose (Isotec) as the carbon source and $^{15}NH_4Cl$ or $(^{15}NH_4)_2SO_4$ (Isotec) as the nitrogen source (McIntosh and Dahlquist, 1990). A typical yield is 89 mg of purified protein from 1 l of cell growth, obtained in ^{13}C- and ^{15}N-enriched minimal medium.

For assignment and structure determination, 14T was dialyzed against NMR buffer (50 mM NaH_2PO_4, 100 mM NaCl and 0.1 mM Na-azide, pH 4.15) and concentrated to a sample volume of approximately 500 µl. D_2O was added to 7%. For some samples, the salts for the NMR buffer were dissolved in 99.9% D_2O and the solvent was exchanged by ultrafiltration. For the hydrogen exchange experiments, a ^{15}N-labeled sample in NMR buffer (pH 4.15) was lyophilized. At time zero, the lyophilized sample was redissolved in 99.98% D_2O. For the pH and calcium titrations, ^{15}N-labeled villin 14T was exchanged into 50 mM deuterated acetate buffer, 100 mM NaCl, 0.1 mM Na-azide and 7% D_2O by ultrafiltration. Sample concentrations ranged from 1.65 to 6.72 mM, depending on the availability of material. Samples were stored in solution at 277 K.

NMR spectroscopy

NMR spectra of villin 14T were acquired on Bruker AMX 500 and AMX 600 spectrometers at 298 K. Unless otherwise noted, sign discrimination was achieved with time-proportional phase incrementation (TPPI), the water suppression technique was presaturation during the recycle delay, and ^1H carriers were placed on the water line. Spectra were processed and plotted with the FELIX software package (formerly Hare Research Inc., now Biosym Technologies, San Diego, CA). In general, processing involved multiplication of the free induction decays by a shifted, sine-squared apodization function, zero-filling to enhance resolution, and Fourier transformation. When appropriate, processing also included removal of the low-frequency component of the fid to remove residual water (Marion et al., 1989c) and linear prediction of additional points in the indirectly acquired dimensions to enhance resolution (Olejniczak and Eaton, 1990).

For sequential assignments, the HNCA (Kay et al., 1990) and HN(CO)CA (Bax and Ikura, 1991) experiments were run on fully ^{13}C- and ^{15}N-labeled 14T in 93% H_2O/7% D_2O at 5.70 mM. The experiments were implemented with constant time in ^{15}N (Grzesiek and Bax, 1992), GARP decoupling of ^{15}N during acquisition, and spin-lock pulses for water suppression (Messerle et al., 1989). The HNCA spectrum was acquired with spectral widths of 33.15, 44.77 and 16.02 ppm in F_1 (^{15}N), F_2 (^{13}C) and F_3 (^1H), respectively, and with 53 real points in t_1, 128 real points in t_2 and 512 complex points in t_3; 32 scans per point. The carriers were set to 118.0 ppm for ^{15}N and 50.0 ppm for ^{13}C. Parameters were the same for the HN(CO)CA experiment, except that only 38 real points were collected for t_1 and the ^{15}N carrier was set to 116.0 ppm.

Sequential assignments were confirmed with experiments linking residues through the carbonyl chemical shifts. Interresidue connectivities were obtained by means of an HNCO experiment (Grzesiek and Bax, 1992), implemented with gradient water suppression (Kay et al., 1993) and nonlinear random sampling in the ^{15}N dimension (Barna et al., 1987; Schmieder et al., 1994). It was acquired on the same sample used for the HNCA experiment. The spectral widths were 50.13, 16.56 and 10.41 ppm in F_1 (^{15}N), F_2 (^{13}C) and F_3 (^1H), respectively. 23 of 83 complex points were sampled in t_1, 256 real points in t_2 and 512 complex points in t_3, with 16 scans per point. The carriers were set to 116.0 ppm for ^{15}N and 170.0 ppm for ^{13}C. Intraresidue connectivities were

obtained by means of an HCACO experiment (Powers et al., 1991), implemented with a spin-lock pulse for water suppression and a combination of DANTE pulses and carrier jumping to excite aliphatic or carbonyl carbons selectively. The sample was fully ^{13}C,^{15}N-labeled 14T in D_2O at 4.36 mM. The HCACO spectrum was acquired with spectral widths of 39.76, 39.76 and 10.00 ppm in F_1 ($^{13}C^{\alpha}$), F_2 ($^{13}C'$) and F_3 (^1H), respectively, and with 36 complex points in t_1, 128 complex points in t_2 and 1024 complex points in t_3; 16 scans per point. The carriers were set to 116.0 ppm for ^{15}N and 50.0 and 170.0 ppm for ^{13}C. Sign discrimination in the indirect dimensions of these experiments was achieved by the TPPI-States method.

Two 3D correlation experiments were the basis for side-chain assignments. A ^{15}N TOCSY-HMQC experiment (Marion et al., 1989a), with presaturation of water during the recycle delay, followed by SCUBA recovery (Brown et al., 1988), and additional presaturation during the refocusing delays, was run on ^{15}N-labeled 14T at 1.65 mM in H_2O. The spectral width was 18.18 ppm for both F_1 (^1H) and F_3 (^1H) and 34.53 ppm for F_2 (^{15}N), with 256 real $\times$ 33 real $\times$ 1024 complex points ($t_1 \times t_2 \times t_3$) and 12 scans per point. The ^{15}N carrier was set to 117.16 ppm. The ^{13}C heteronuclear cross-polarization experiment ('HEHOHEHAHA', Majumdar et al., 1993) was run on the fully ^{13}C- and ^{15}N-labeled sample in D_2O at 4.36 mM. The DISPSI-3 spin-lock sequence was cycled once (6.1 ms) for transfer between ^1H and ^{13}C and three times (18.3 ms) for ^{13}C-to-^{13}C transfer. The spectral widths were 6.67 ppm in F_1 (^1H), 69.90 ppm in F_2 (^{13}C) and 20.83 ppm in F_3 (^1H), with 128 real $\times$ 92 real $\times$ 512 complex points and 8 scans per point. The ^1H carriers were set to 2.28 ppm, although the F_3 (^1H) carrier was shifted to the water line for presaturation, and the ^{13}C carrier was positioned at 36 ppm.

NOE restraints were based on experiments including 3D ^{15}N- and ^{13}C-NOESY-HMQC sequences (Marion et al., 1989a,b). The ^{15}N spectrum was recorded with presaturation and SCUBA to suppress water. The mixing time was set to 150 ms. The sample, spectral widths and carriers were as in the ^{15}N-TOCSY-HMQC experiment. There were 128 real $\times$ 51 real $\times$ 1024 complex points ($t_1 \times t_2 \times t_3$) and 16 scans per point. The ^{13}C spectrum was recorded on the same sample as that used for the HEHOHEHAHA experiment, with a mixing time of 100 ms and sign discrimination by States-TPPI in the ^{13}C dimension. The spectral widths were 9.60 ppm in F_1 (^1H), 80 ppm in F_2 (^{13}C) and 14.08 ppm in F_3 (^1H), with 256 real $\times$ 36 complex $\times$ 512 complex points and 8 scans per point. The carrier for ^{13}C was set at 36 ppm. NOE cross peaks were only loosely quantitated by counting plotted contour levels.

Interpretation of the 3D data was facilitated by reference to heteronuclear correlation spectra, acquired as HSQC (Bodenhausen and Ruben, 1980). The reference ^{15}N HSQC spectrum was acquired on the 1.65-mM, ^{15}N-labeled sample with 300 real points in t_1 and 1024 complex points in t_2, at 8 scans per point. The spectral widths were 59.43 ppm in F_1 (^{15}N) and 14.08 ppm in F_2 (^1H) and the ^{15}N carrier was positioned at 108 ppm. A higher resolution ^{15}N spectrum was acquired on the same sample to determine $^3J_{H^NH^{\alpha}}$. The parameters were 512 real points $\times$ 2048 complex points at 64 scans per point, spectral widths of 40 and 8.00 ppm, and carriers at 9.35 ppm for ^1H and 115.1 ppm for ^{15}N. Spin-lock pulses were used for water suppression (Messerle et al., 1989). The reference ^{13}C HSQC spectrum was acquired on 4.36 mM ^{13}C,^{15}N-labeled 14T in D_2O with 918 real points in t_1 and 1024 complex points in t_2 at 48 scans per point, spectral widths of 79.53 ppm for F_1 (^{13}C) and 15.15 ppm for F_2 (^1H) and the ^{13}C carrier at 35 ppm. Spin-lock pulses were used for water suppression. The parameters for the acquisition of a ^{13}C HSQC spectrum on the 10% ^{13}C-labeled sample (6.72 mM) were virtually the same.

3D data sets were also supplemented with 2D homonuclear data. COSY (Piantini et al., 1982), TOCSY (Braunschweiler and Ernst, 1983) and NOESY spectra were acquired on unlabeled 14T at 2.85 mM in H_2O. Data were acquired with 1024 complex points in t_2 and spectral widths of 14.08 ppm in both dimensions. The COSY was double-quantum filtered with 700 real points in t_1 and 48 scans per point. The TOCSY was run with clean delays and a spin-lock time of 60 ms, with 670 real points in t_1 and 64 scans per point. The NOESY had a mixing time of 150 ms, 512 real points in t_1 and 48 scans per point. TOCSY and NOESY spectra were also acquired on a 3.68-mM sample in D_2O. Data were collected with 608 real points in t_1 and 1024 complex points in t_2 and spectral widths of 14.08 ppm in both dimensions. The TOCSY in D_2O used a DIPSI-2 spin-lock; mixing times of 30, 55 and 80 ms were co-added, and 64 scans per point were acquired. The NOESY in D_2O had a 100-ms mixing time and 160 scans per point.

To measure coupling constants, HNHA (Vuister and Bax, 1993) and HNHB spectra (Archer et al., 1991) were acquired on a 1.65-mM sample of ^{15}N-labeled villin 14T. Both experiments featured constant-time evolution for ^{15}N and sign discrimination by TPPI-States in the indirect dimensions. In both experiments, the spectral widths were 50.13 ppm in F_1 (^{15}N), 11.90 ppm in F_2 (^1H) and 16.66 ppm in F_3 (^1H); the ^{15}N carrier was placed at 116 ppm. The HNHA was run with presaturation for water suppression and $31 \times 64 \times 1024$ complex points ($t_1 \times t_2 \times t_3$), with 16 scans per point. The HNHB used WATERGATE (Sklenar et al., 1993) as the water suppression scheme. Data were acquired as $97 \times 64 \times 512$ complex points with 8 scans per point.

Coupling constants and stereospecific assignments

The α-proton to amide proton scalar coupling constants ($^3J_{HN_H\alpha}$) were determined from cross-peak splittings in the proton dimension of a ^{15}N HSQC spectrum and confirmed with data from the HNHA experiment (Vuister and Bax, 1993). Stereospecific assignments for β-methylene protons were based on the coupling constant $^3J_{H\alpha_H\beta}$ between the α- and β-protons, classified as large or small from the COSY data, and the coupling constant $^3J_{NH\beta}$ between the amide nitrogen and β-proton, classified as large or small from the HNHB experiment (Archer et al., 1991). Stereospecific assignments for methyl groups of valine and leucine were obtained from the ^{13}C HSQC spectrum acquired on the 10% ^{13}C-labeled sample (Neri et al., 1989; Senn et al., 1989; Szyperski et al., 1992).

Hydrogen exchange experiments

The sample was lyophilized from NMR buffer (pH 4.15) and then redissolved in D_2O at time zero. ^{15}N HSQC spectra were recorded with 8 scans and 128 t_1 increments. Experiments were started at times 11, 30, 50, 69, 89, 108, 128, 157, 186, 216, 249, 279, 309, 338, 367, 464, 524, 583, 642, 702, 761, 820, 880, 939, 998, 1058, 1117, 1176, 1236, 1295 and 9920 min, sampling over one 24-h period with an additional experiment one week later. Temperature during exchange was maintained at 298 K. For each residue, peak volumes were measured in FELIX, and the natural logarithms of the peak volumes were plotted as a function of time. This representation gives a line with slope equal to the negative of the exchange rate for that residue. A least-squares fit to this line gives the slope with its standard deviation, and therefore the exchange rate and an estimate of its error. This error is estimated as twice the standard deviation for a 95% confidence level.

pH and calcium titration experiments

Local changes in the protein as a function of pH and Ca^{2+} concentration were monitored with ^{15}N HSQC experiments, run with 8 scans and 256 t_1 increments. First the pH of the sample was

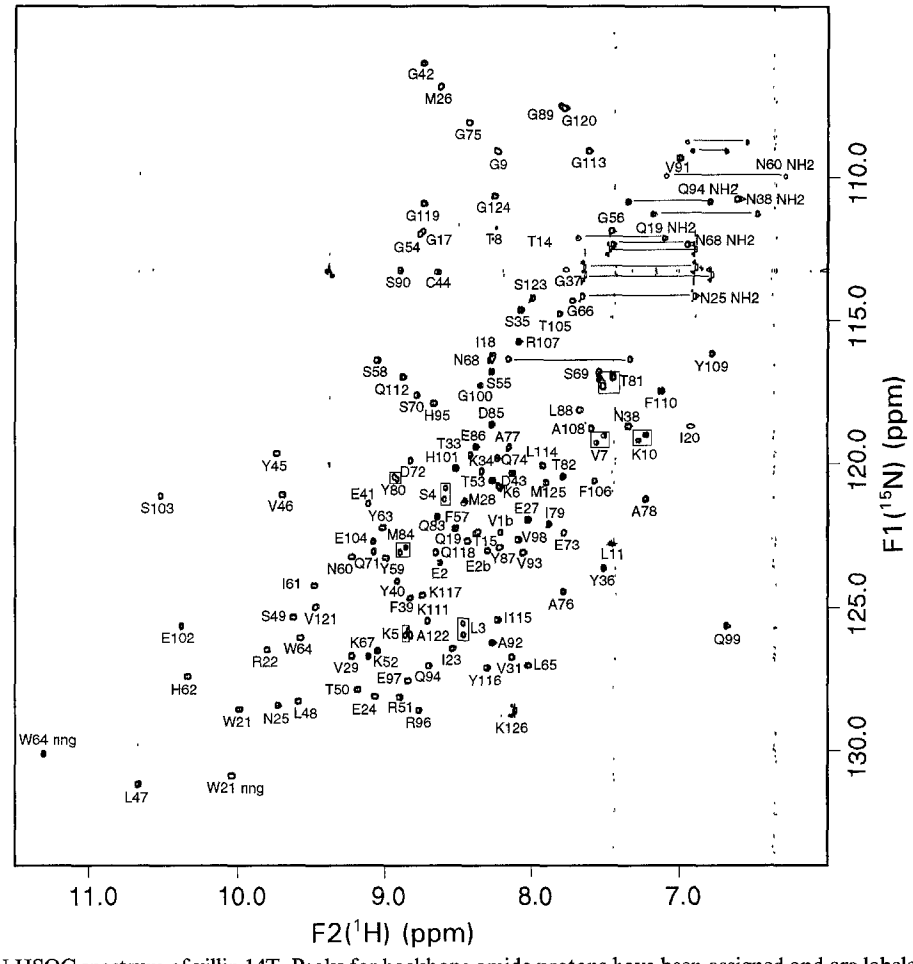

Fig. 1. ^{15}N HSQC spectrum of villin 14T. Peaks for backbone amide protons have been assigned and are labeled with the one-letter code for the amino acid type, followed by the position in the sequence. Tryptophan pyrrole protons have also been labeled. Peaks for side-chain amide protons are connected by horizontal lines and labeled where the assignments are known. Residues 1 and 2 each have two distinct peaks; the second set of peaks is labeled '1b' and '2b'. Pairs of nearby peaks which correspond to the same residue are enclosed in boxes.

increased from 4.10 to 6.91 in steps of approximately 0.2 pH units. Then small volumes of $CaCl_2$, diluted with the acetate buffer, were added to the sample. Calcium concentrations varied from 0.0 to 50.0 mM, in steps starting at 0.2 mM and increasing gradually to 10.0 mM. The dissociation constants for Ca^{2+} binding have been calculated (Markus et al., 1994).

Structure calculations

The structures were calculated with the distance geometry algorithm, implemented in the program DGII (Havel, 1991), used as part of the INSIGHT II software package (Biosym Technologies, San Diego, CA). Details of the structure calculations have been presented elsewhere (Markus et al., 1994).

RESULTS

Assignment strategy

In general, spectra of villin 14T were of good quality and displayed a high signal-to-noise ratio, as demonstrated in the higher resolution ^{15}N HSQC spectrum in Fig. 1. Since the chemical shift dispersion for the amide protons and nitrogens is generally good, initially each peak in the ^{15}N HSQC was assumed to correspond to one residue's spin system. Prior to sequential assignments, spin systems were partially classified and peaks corresponding to side-chain amides and tryptophan ring pyrroles were identified on the basis of the ^{15}N TOCSY-HMQC.

Sequential connectivities were based on the HNCA and HN(CO)CA experiments. The HNCA correlates each amide proton and nitrogen to its intraresidue and, to some extent, neighboring interresidue α-carbons. The HN(CO)CA correlates the amide proton and nitrogen with the neighboring interresidue α-carbon. These experiments gave sequential connectivities for 90% of the residues. These connectivities were confirmed and extended with the HCACO and HNCO experiments. The HCACO correlates the intraresidue carbonyl carbon with its α-proton and carbon, while the HNCO correlates the carbonyl with the neighboring sequential amide proton and nitrogen. This pair of experiments gave sequential connectivities for about 94% of the residues. The main improvement occurred in the vicinity of the proline residues. Since proline lacks an amide proton, the HNCA, HN(CO)CA and HNCO experiments do not give information for this amino acid. For sequential assignment, this introduces a gap of two connectivities at each proline for the HNCA/HN(CO)CA experiments, but only one for the HCACO/HNCO pair. However, the HNCA/HN(CO)CA pair is more straightforward to interpret. The α-carbon chemical shifts in 14T are distributed over 24.5 ppm (17.4 ppm excluding glycine), while the carbonyl chemical shifts are distributed over only 10.2 ppm, which leads to more ambiguities in the sequential assignments. Classification of the residues was sufficient to position the connected residues within the known sequence of the protein. Sequential assignments were extended to cover 98% of the backbone, based on NOE data (Wüthrich, 1986). Backbone assignments are complete, except for the nitrogen chemical shifts of the three proline residues, the amide proton and nitrogen chemical shifts for the N-terminal valine, and assignments for Asp^{12} and Lys^{13}. Sequential connectivities in 14T are summarized in Fig. 2.

Amide nitrogen-to-proton cross peaks for Asp^{12} and Lys^{13} have not been identified in the ^{15}N HSQC spectrum. Cross peaks assigned to the neighboring residues Leu^{11} and Thr^{14} are noticeably broader than the majority of the peaks (see Fig. 1), which suggests that the cross peaks for Asp^{12} and Lys^{13} may be broadened beyond detection. These residues are located in a region between the putative N-terminal α-helix and strand β1 of the central β-sheet. The local broadening may be the result of an exchange process at an intermediate rate on the NMR time scale; the exchange process could involve the chemical exchange of the amide protons or a physical exchange between conformations. Spin systems starting from the α-protons have been tentatively identified in the 2D TOCSY spectra for Asp^{12} and Lys^{13}. However, without the amide cross peaks, these assignments have not been confirmed due to overlap in the spectra and lack of sequential connectivities. As the structure is refined and the relaxation properties of 14T are characterized, we hope to understand this region of the protein better.

To extend the side-chain assignments, a ^{13}C heteronuclear cross-polarization experiment (HEHOHEHAHA) was analyzed with supporting information from the ^{13}C HSQC spectrum.

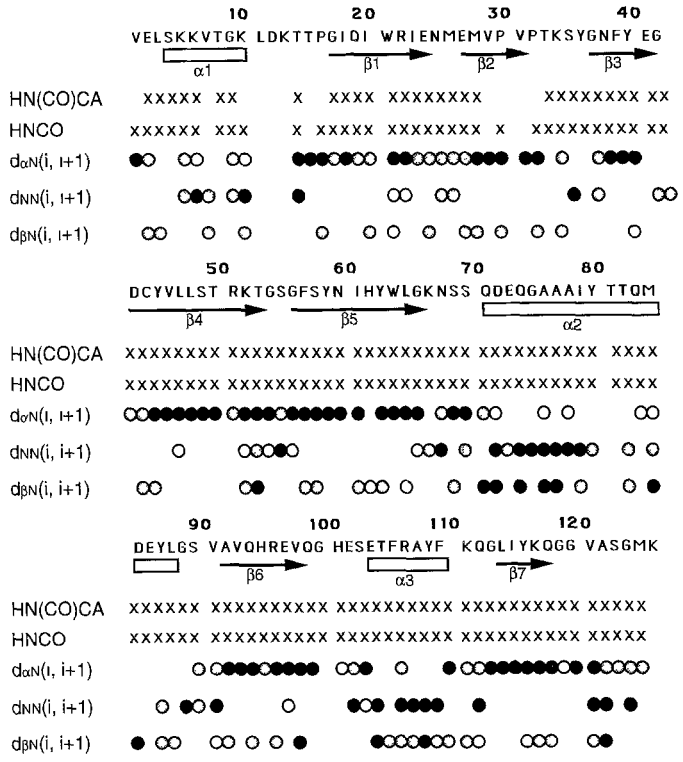

Fig. 2. Sequential connectivities for villin 14T. In the top row, the numbers represent the sequence position. In the second row, the letters represent the one-letter code for the amino acid sequence. Letters are grouped in sets of 10 for clarity. Beneath the sequence, the elements of secondary structure are summarized with symbols. Open rectangles represent α-helices and arrows represent strands of β-sheet. The elements of secondary structure are also labeled. The row labeled HN(CO)CA contains an 'x' for every residue which can be connected to the next residue by an assigned cross peak in the HN(CO)CA spectrum. The row labeled HNCO contains an 'x' for every residue which can be connected to the next residue by an assigned cross peak in the HNCO spectrum. The rows labeled $d_{\alpha N}(i, i+1)$, $d_{NN}(i, i+1)$ and $d_{\beta N}(i, i+1)$ summarize the sequential NOE cross peaks. Strong cross peaks are represented by filled circles, medium cross peaks by dotted circles, and weak cross peaks by open circles.

Aromatic protons were assigned primarily from the 2D TOCSY data sets in D_2O and H_2O. Aromatic carbon chemical shifts were assigned for unique aromatic proton chemical shifts, based on a ^{13}C CT-HSQC. The HNHB experiment, acquired to measure $^3J_{NH\beta}$, resolved ambiguities or provided assignments for six β-protons. Assignments are complete for 94 of the 126 residues, including chemical shifts for nitrogens, protons and proton-attached carbons, but excluding the carbons of the aromatic rings, the terminal amines of arginine and lysine, and the imidazole amines of the histidines. Measurements of the α- to β-proton coupling constant ($^3J_{H\alpha H\beta}$) and the amide nitrogen to β-proton coupling constant ($^3J_{NH\beta}$) led to stereospecific assignments for 35 of the 82 pairs of β-methylene protons. The ^{13}C HSQC spectrum acquired on the 10% ^{13}C-labeled sample provided stereospecific assignments of the methyl groups in eight of the nine valine residues and five of the seven leucines. The assignments are summarized in Table 1.

Although initially each peak in the ^{15}N HSQC was assumed to correspond to a different spin

TABLE 1
^{15}N, ^{13}C AND ^{1}H CHEMICAL SHIFT ASSIGNMENTS FOR VILLIN 14T AT pH 4.15 AND 25 °C

Residue	N	CO	C^{α}	C^{β}	Other
V1		168.2	56.1 (3.87)	28.0 (2.08)	$C^{\gamma R}$ 16.3 (0.83); $C^{\gamma S}$ 14.0 (0.55)
V1b	122.2 (8.22)	171.1	57.6 (4.21)	28.1 (1.94)	$C^{\gamma R}$ 16.9 (0.64); $C^{\gamma S}$ 15.2 (0.56)
E2	123.4 (8.63)	171.6	50.4 (4.76)	– (1.95)	C^{γ} – (2.34)
E2b	122.8 (8.31)	171.5	50.1 (4.75)	– (2.00, 1.86)	C^{γ} – (2.34)
L3	125.9 (8.47)	173.2	50.5 (4.25)	38.2 (1.53, 1.44)^{S,R}	C^{γ} 21.9 (1.59); C^{δ} 20.3 (0.59)
S4	120.9 (8.56)	172.3	53.0 (4.50)	60.1 (4.28, 3.90)	
K5	125.9 (8.87)	175.6	53.1 (4.48)	27.6 (1.85)	C^{γ} 20.6 (1.52, 1.48); C^{δ} 24.4 (1.70); C^{ε} 37.4 (3.05)
K6	120.8 (8.23)	174.9	53.9 (4.14)	28.6 (1.86, 1.81)	C^{γ} – (1.54, 1.48); C^{ε} – (3.03)
V7	119.2 (7.56)	174.6	60.2 (3.90)	27.6 (1.96)	$C^{\gamma R}$ 16.2 (0.37); $C^{\gamma S}$ 17.6 (0.77)
V7b	119.0 (7.52)	174.6	60.2 (3.90)	27.6 (1.96)	$C^{\gamma R}$ 16.2 (0.34); $C^{\gamma S}$ 17.6 (0.77)
T8	112.1 (8.27)	173.0	60.5 (3.52)	63.0 (3.73)	C^{γ} 17.6 (0.62)
G9	109.1 (8.24)	171.6	41.9 (3.98, 3.88)		
K10	119.1 (7.28)	171.3	51.2 (4.48)	28.3 (2.13, 1.91)	C^{γ} 20.3 (1.58, 1.53); C^{δ} 24.1 (1.77); C^{ε} 37.4 (3.07)
L11	122.8 (7.49)	172.5	51.4 (4.32)	37.3 (1.78, 1.62)	C^{γ} 22.3 (1.70); C^{δ} 20.6 (0.77)
D12					
K13					
T14	112.1 (8.05)	170.4	56.3 (3.89)	64.8 (4.15)	C^{γ} 16.7 (0.85)
T15	122.4 (8.37)	168.8	55.4 (4.63)	65.3 (3.97)	C^{γ} 16.7 (1.23)
P16		172.0	58.6 (4.23)	24.2 (2.38, 1.86)	C^{γ} – (2.07); C^{δ} 46.8 (4.14, 3.85)
G17	111.9 (8.74)	169.1	39.8 (4.68, 3.82)		
I18	116.3 (8.28)	171.4	54.4 (5.42)	37.0 (1.39)	C^{γ} 21.7 (1.32, 0.94); $C^{\gamma m}$ 13.4 (0.37); C^{δ} 9.6 (0.34)
Q19	122.6 (8.44)	170.4	50.3 (4.59)	– (1.60, 1.40)	C^{γ} 31.0 (2.23, 2.05); N^{ε} 112.1 (7.68, 7.11)
I20	118.7 (6.94)	170.6	55.8 (5.08)	36.2 (1.12)	C^{γ} 22.9 (0.69, 0.55); $C^{\gamma m}$ 14.4 (1.01); C^{δ} 9.8 (0.20)
W21	128.5 (9.99)	170.3	53.3 (5.30)	29.2 (3.03, 2.82)^{R,S}	$C^{\delta 2}$ 119.6 (6.49); $C^{\varepsilon 3}$ – (7.70); $C^{\zeta 2}$ – (7.22); $C^{\zeta 3}$ – (6.81); C^{η} – (6.81); $N^{\varepsilon 1}$ 131.2 (10.68)
R22	126.6 (9.81)	171.5	49.8 (4.48)	– (1.91)	C^{γ} – 0; C^{δ} – (3.38, 3.12); N^{ε} 84.8 (7.80)
I23	126.4 (8.55)	172.0	54.5 (4.86)	30.4 (2.11)	C^{γ} 23.3 (1.34, 1.30); $C^{\gamma m}$ 13.1 (0.92); C^{δ} 7.2 (0.73)
E24	128.1 (9.07)	172.5	49.7 (4.74)	26.8 (2.13, 1.92)	C^{γ} 29.3 (2.31)
N25	128.4 (9.73)	171.1	50.1 (4.41)	32.8 (3.02, 2.79)^{S,R}	N^{δ} 114.2 (7.66, 6.90)
M26	106.8 (8.63)	171.4	52.2 (3.86)	25.0 (2.54, 2.20)^{S,R}	C^{γ} 28.4 (2.63, 2.38); C^{ε} 12.7 (1.97)
E27	122.0 (8.03)	171.4	50.0 (4.76)	26.7 (2.04, 2.02)	C^{γ} 29.3 (2.49, 2.43)
M28	121.3 (8.46)	171.7	51.6 (4.28)	27.1 (1.42, 1.20)	C^{γ} – (0.91, 0.87); C^{ε} 11.3 (0.70)
V29	126.7 (9.24)	170.5	54.9 (4.87)	30.3 (2.21)	$C^{\gamma R}$ 16.1 (1.08); $C^{\gamma S}$ 16.4 (0.98)
P30		173.3	59.4 (4.42)	27.7 (2.27)	C^{δ} 46.8 (4.16, 3.97); also (2.14, 1.86)
V31	126.6 (8.14)	170.6	55.2 (4.49)	29.6 (1.97)	$C^{\gamma R}$ 16.1 (1.19); $C^{\gamma S}$ 19.7 (1.20)
P32		175.1	58.6 (4.55)	27.7 (2.40, 1.87)	C^{γ} 23.5 (2.15, 2.05); C^{δ} 46.7 (4.02, 3.74)
T33	119.7 (8.42)	174.1	60.8 (2.74)	63.3 (3.72)	C^{γ} 17.5 (1.01)
K34	120.3 (8.35)	173.5	53.5 (4.12)	27.2 (1.81)	C^{γ} 20.1 (1.40); C^{δ} 24.6 (1.65); C^{ε} 37.0 (2.93)
S35	114.7 (8.08)	170.5	53.3 (4.50)	60.1 (4.02, 3.88)	
Y36	123.6 (7.52)	173.4	52.9 (4.15)	31.8 (3.33, 2.90)	
G37	113.2 (7.77)	167.3	40.3 (4.09, 2.18)		
N38	118.7 (7.35)	170.9	46.7 (5.09)	34.6 (2.77, 1.89)^{S,R}	N^{δ} 110.8 (6.63)
F39	124.7 (8.83)	171.1	52.0 (4.02)	37.2 (1.89, 1.70)^{S,R}	C^{δ} 127.4 (5.52); C^{ε} 124.0 (5.95); C^{ζ} – (6.41)
Y40	124.1 (8.92)	174.4	54.7 (4.98)	33.4 (3.44, 3.36)	C^{δ} – (7.11); C^{ε} – (6.78)
E41	121.4 (9.12)	173.4	54.1 (4.56)	– (2.25, 1.59)	C^{γ} 30.6 (2.85, 2.72)

TABLE 1 (continued)

Residue	N	CO	C^{α}	C^{β}	Other
G42	106.0 (8.74)	169.5	40.3 (3.96, 3.68)		
D43	120.3 (8.14)	170.8	48.6 (5.66)	– (3.16, 2.99)^{S,R}	
C44	113.3 (8.64)	170.0	53.3 (6.14)	27.6 (3.10, 2.76)^{R,S}	
Y45	119.6 (9.74)	171.6	52.2 (5.90)	– (3.30, 3.21)^{S,R}	C^{δ} 129.7 (7.47); C^{ε} – (7.31)
V46	121.1 (9.71)	169.6	57.8 (5.12)	31.7 (2.02)	$C^{\gamma R}$ 17.0 (1.04); $C^{\gamma S}$ 17.5 (1.09)
L47	130.9 (10.04)	170.7	49.4 (5.79)	42.8 (1.99, 1.79)^{S,R}	C^{γ} 23.0 (1.60); $C^{\delta R}$ 25.0 (0.69); $C^{\delta S}$ 22.3 (0.55)
L48	128.3 (9.59)	171.8	49.3 (5.48)	42.3 (2.24, 1.67)^{S,R}	C^{γ} 23.2 (1.70); $C^{\delta R}$ 19.7 (1.07); $C^{\delta S}$ 22.1 (1.08)
S49	125.3 (9.63)	170.9	51.3 (5.36)	58.7 (4.00, 3.34)^{R,S}	
T50	127.9 (9.19)	170.9	57.6 (4.94)	65.3 (4.25)	C^{γ} 18.0 (0.89)
R51	128.1 (8.90)	170.9	49.7 (4.83)	29.2 (1.78, 1.71)	C^{γ} 23.4 (1.63); C^{δ} 38.8 (3.20); N^{ε} 85.4 (7.18)
K52	126.5 (9.06)	172.3	51.9 (4.38)	29.2 (1.88, 1.53)^{R,S}	C^{γ} 20.4 (1.27, 1.13); C^{δ} 24.6 (1.56); C^{ε} 37.3 (2.91)
T53	120.6 (8.27)	171.4	55.1 (4.62)	66.1 (4.25)	C^{γ} 16.8 (1.05)
G54	112.0 (8.76)	171.4	42.2 (3.98, 3.80)		
S55	116.8 (8.28)	170.3	53.2 (4.56)	59.2 (3.94, 3.84)	
G56	111.9 (7.47)	168.6	40.5 (4.06, 3.84)		
F57	122.2 (8.52)	171.5	52.7 (5.26)	38.8 (2.63, 2.45)^{R,S}	C^{δ} – (7.03); C^{ε} – (7.25); C^{ζ} – (7.33)
S58	116.4 (9.06)	170.0	52.2 (4.69)	60.7 (3.74, 3.65)	
Y59	123.3 (9.00)	172.2	52.1 (5.94)	37.2 (2.97, 2.66)^{S,R}	C^{δ} – (7.21); C^{ε} – (6.88)
N60	123.2 (9.23)	170.2	48.1 (5.76)	39.2 (3.08, 2.88)^{S,R}	N^{δ} 109.9 (7.09, 6.31)
I61	124.2 (9.47)	171.8	55.3 (5.69)	36.4 (1.70)	C^{γ} 22.9 (1.62); $C^{\gamma m}$ 15.8 (1.20); C^{δ}10.6 (0.85)
H62	127.4 (10.34)	170.6	48.6 (6.15)	27.8 (3.55, 3.28)^{R,S}	
Y63	122.2 (9.02)	168.5	50.1 (6.15)	34.8 (3.46, 2.94)^{S,R}	C^{δ} – (7.13); C^{ε} – (6.82)
W64	126.1 (9.58)	172.2	51.9 (5.40)	29.1 (3.29, 2.38)	$C^{\delta 2}$ 122.2 (5.93); $C^{\varepsilon 3}$ 117.2 (7.86); $C^{\zeta 2}$ 108.0 (7.09); $C^{\zeta 3}$ – (7.68); C^{η} – (6.84); $N^{\varepsilon 1}$ 130.1 (11.30)
L65	127.0 (8.03)	171.5	47.9 (5.01)	– (1.74, 1.07)^{R,S}	C^{γ} 21.7 (1.77); $C^{\delta R}$ 21.0 (0.86); $C^{\delta S}$ 19.8 (1.10)
G66	114.3 (7.72)	174.4	42.6 (4.12, 3.58)		
K67	126.7 (9.12)	173.2	54.3 (4.07)	28.3 (1.71, 1.35)^{R,S}	C^{γ} 19.2 (1.35, 1.15); C^{δ} 25.0 (1.56); C^{ε} – (2.92)
N68	116.3 (8.28)	171.3	47.3 (5.26)	34.8 (3.27, 2.20)^{R,S}	N^{δ} 112.4 (7.47, 6.96)
S69	116.9 (7.55)	170.9	53.7 (4.49)	61.3 (3.99, 3.71)^{S,R}	
S70	117.6 (8.79)	172.2	52.5 (4.68)	60.7 (4.34, 4.07)^{S,R}	
Q71	123.0 (9.08)	175.1	54.9 (3.82)	24.0 (2.14)	C^{γ} 29.5 (2.47)
D72	119.9 (8.83)	175.2	52.3 (4.40)	34.4 (2.76, 2.68)^{R,S}	
E73	122.4 (7.78)	174.3	54.6 (4.14)	– (2.39, 2.33)	C^{γ} 30.3 (2.73, 2.60)
Q74	119.8 (8.24)	176.8	54.3 (4.27)	– (2.13)	
G75	108.1 (8.44)	172.5	42.3 (3.90, 3.81)		
A76	124.5 (7.79)	174.6	50.3 (3.80)	13.4 (1.41)	
A77	119.4 (8.16)	175.4	51.2 (3.84)	13.3 (1.56)	
A78	121.2 (7.23)	176.6	50.4 (2.94)	13.7 (1.30)	
I79	122.1 (7.89)	175.4	60.3 (3.69)	33.2 (1.48)	C^{γ} 24.6 (1.54, 1.03); $C^{\gamma m}$ 13.4 (0.63); C^{δ} 8.5 (0.67)
Y80	120.6 (8.93)	175.4	56.7 (4.21)	33.2 (2.98, 2.73)^{S,R}	C^{δ} – (6.75); C^{ε} – (6.40)
T81	116.9 (7.55)	172.4	64.1 (3.79)	63.1 (4.20)	C^{γ} 16.3 (1.28)
T82	120.5 (7.80)	173.1	62.5 (3.96)	64.2 (4.35)	C^{γ} 17.2 (1.27)
Q83	121.8 (8.65)	176.2	54.7 (4.08)	– (2.12)	
M84	123.1 (8.90)	173.4	54.9 (3.76)	28.3 (2.15, 2.05)	C^{γ} 27.8 (2.32); C^{ε} 12.1 (1.33)
D85	118.6 (8.28)	174.8	52.0 (4.14)	33.9 (3.38, 2.76)	
E86	119.4 (8.39)	176.2	54.6 (4.05)	– (2.24, 2.10)	

TABLE 1 (continued)

Residue	N	CO	C^{α}	C^{β}	Other
Y87	122.9 (8.22)	173.5	57.0 (4.12)	33.9 (3.14, 3.03)	C^{δ} – (6.92); C^{ε} – (6.74)
L88	118.1 (7.68)	173.2	50.1 (4.05)	– (1.74, 1.35)^{R,S}	C^{γ} 21.7 (1.77); $C^{\delta R}$ 21.4 (0.32); $C^{\delta S}$ 17.4 (0.42)
G89	107.6 (7.79)	171.6	41.3 (4.26, 3.85)		
S90	113.2 (8.90)	171.2	55.2 (3.98)	56.6 (4.15, 4.07)	
V91	109.3 (7.01)	172.9	56.0 (4.60)	27.7 (2.70)	$C^{\gamma R}$ 16.9 (1.05); $C^{\gamma S}$ 13.7 (1.07)
A92	126.2 (8.27)	172.9	46.6 (5.04)	16.4 (1.31)	
V93	123.1 (8.06)	172.1	57.9 (4.18)	27.8 (2.20)	$C^{\gamma R}$ 17.1 (0.71); $C^{\gamma S}$ 16.8 (1.08)
Q94	127.0 (8.71)	172.5	50.5 (5.27)	– (2.01, 1.96)	C^{γ} – (2.34); N^{ε} 110.9 (6.80, 7.36)
H95	117.9 (8.67)	168.6	50.1 (4.80)	27.7 (3.19, 2.69)	$C^{\varepsilon 1}$ 131.6 (8.78); $C^{\delta 2}$ 115.4 (6.33)
R96	128.6 (8.77)	171.3	51.1 (3.28)	– (1.66)	C^{γ} – (1.09, 0.92); C^{δ} 38.9 (3.16); N^{ε} 85.3 (7.14)
E97	127.5 (8.85)	170.3	48.4 (5.04)	– (1.60, 1.35)^{R,S}	
V98	122.6 (8.09)	171.5	56.1 (3.73)	29.2 (1.70)	$C^{\gamma R}$ 16.4 (0.82); $C^{\gamma S}$ 16.9 (0.74)
Q99	125.6 (6.69)	172.9	53.5 (3.80)		
G100	117.3 (8.36)	170.5	40.5 (4.17, 3.89)		
H101	120.1 (8.52)	171.9	49.4 (5.01)	24.7 (3.56, 2.60)^{R,S}	$C^{\varepsilon 1}$ 131.5 (8.61); $C^{\delta 2}$ 115.6 (7.11)
E102	125.6 (10.38)	173.4	54.1 (4.40)	– (1.90)	
S103	121.1 (10.52)	171.5	54.1 (4.34)	59.9 (4.53, 4.44)^{R,S}	
E104	122.7 (9.08)	175.5	54.1 (4.00)	23.5 (2.13)	C^{γ} 30.9 (2.48)
T105	114.8 (7.82)	170.4	61.4 (3.52)	64.4 (3.85)	C^{γ} 17.2 (1.07)
F106	120.6 (7.58)	173.1	54.8 (3.75)	34.9 (3.08, 2.95)^{S,R}	C^{δ} 126.8 (6.69); C^{ε} – (6.89); C^{ζ} – (6.41)
R107	115.8 (8.09)	175.2	55.6 (3.80)	25.4 (1.91)	C^{γ} 15.8 (1.63); C^{δ} 38.8 (3.30, 3.20); N^{ε} 84.9 (6.90)
A108	118.8 (7.60)	175.3	48.6 (4.02)	13.4 (1.26)	
Y109	116.2 (6.79)	172.4	53.1 (4.18)	31.9 (2.14, 1.62)^{S,R}	C^{δ} 128.2 (6.56); C^{ε} 112.6 (6.04)
F110	117.4 (7.13)	172.7	51.5 (4.67)	34.8 (3.07, 2.66)	C^{δ} 128.5 (6.98); C^{ε} 125.6 (6.22); C^{ζ} 123.2 (6.51)
K111	125.5 (8.71)	174.4	54.4 (4.04)	27.6 (1.88)	C^{γ} 20.7 (1.53, 1.48); C^{δ} 24.5 (1.68); C^{ε} 37.4 (3.02)
Q112	117.0 (8.88)	172.3	50.8 (4.47)	– (2.27, 2.08)	C^{γ} – (2.43)
G113	109.1 (7.62)	168.2	39.6 (4.16, 3.80)		
L114	120.1 (7.93)	172.6	49.8 (4.35)	38.3 (1.40, 0.95)^{R,S}	C^{γ} 22.7 (1.52); $C^{\delta R}$ 21.6 (0.85); $C^{\delta S}$ 21.2 (0.53)
I115	125.4 (8.23)	170.5	55.2 (3.91)	34.8 (1.69)	C^{γ} 22.6 (1.22, 0.92); $C^{\gamma m}$ 13.2 (0.67); C^{δ} 7.8 (0.64)
Y116	127.1 (8.31)	172.9	49.1 (5.76)	– (3.14, 2.94)^{S,R}	C^{δ} 128.0 (7.17); C^{ε} – (6.92)
K117	124.6 (8.75)	172.0	49.2 (4.62)	30.1 (1.55, 0.81)^{S,R}	C^{γ} 20.0 (1.09, 1.00); C^{δ} 23.9 (1.36); C^{ε} 37.0 (2.77)
Q118	123.1 (8.67)	173.0	52.3 (4.48)	25.2 (2.17, 2.12)	C^{γ} 29.8 (2.52)
G119	110.9 (8.74)	169.8	40.2 (4.35, 3.85)		
G120	107.6 (7.79)	170.5	40.1 (4.14, 3.69)		
V121	125.0 (9.47)	174.3	59.9 (3.78)	27.6 (2.06)	C^{γ} 17.0 (0.96)
A122	126.0 (8.80)	174.6	48.7 (4.34)	14.2 (1.46)	
S123	114.2 (8.00)	171.4	53.7 (4.56)	58.3 (4.05, 3.92)	
G124	110.7 (8.26)	170.7	40.9 (4.10, 3.94)		
M125	120.7 (7.91)	172.0	50.8 (4.52)	– (2.00, 1.70)^{R,S}	C^{γ} 27.9 (2.62, 2.55); C^{ε} 12.8 (2.14)
K126	128.6 (8.12)	177.5	53.1 (4.19)	29.1 (1.84, 1.75)	C^{γ} 20.4 (1.70, 1.43); C^{δ} 24.5 (1.68); C^{ε} 37.4 (3.01)

In each column, ^{15}N and ^{13}C chemical shifts are listed first and the corresponding ^{1}H shifts follow in parentheses. For β-protons, stereospecific assignments are indicated by the R and S following the parentheses. ^{1}H chemical shifts are referenced to 3-(trimethylsilyl) propionic acid. ^{15}N chemical shifts are indirectly referenced to ammonia. ^{13}C chemical shifts are referenced to tetramethylsilane.

system, detailed assignments reveal that 12 residues are represented by two peaks in the HSQC. For 10 of these residues, the peaks in the pair are close together (see Leu^{3}, Ser^{4}, Lys^{5}, Val^{7}, Thr^{8}, Lys^{10}, Leu^{11}, Tyr^{80}, Thr^{81} and Met^{84} in Fig. 1) and the duplication was readily identified by the coincidence that both peaks in each pair gave rise to the same type of spin system in the ^{15}N TOCSY-HMQC with nearly identical NOE cross peaks in the ^{15}N NOESY-HMQC. For two residues, the duplicate peaks are well separated and caused confusion early in the assignment process (see Val^{1} and Val^{1b}, Glu^{2} and Glu^{2b} in Fig. 1). Nine of the overrepresented residues are clustered in the N-terminal region of the protein. N-terminal sequencing of villin 14T shows that it exists in two major forms, one starting at Val^{1} and another with the initiator methionine, required for bacterial expression, still intact. Therefore, the differences in the chemical shifts may be due to the presence or absence of this methionine, as observed for recombinant human thioredoxin (Forman-Kay et al., 1989). Note that Val^{1b} has an observable amide proton, which suggests that it represents the form with the initiator methionine. The other overrepresented residues, i.e., Tyr^{80}, Thr^{81} and Met^{84}, lie on the same side of helix α2, facing the putative N-terminal helix α1. So far, every NOE cross peak identified for one form has been identified for the other form as well, suggesting that both peptide sequences fold into a very similar structure. However, it remains possible that the double peaks correspond to different N-terminal conformations of villin 14T. This possibility will be investigated as the structure is refined.

Identification of NOE cross peaks

NOE cross peaks have been assigned in the ^{15}N NOESY-HMQC, ^{13}C NOESY-HMQC and 2D NOESY spectra in H_2O and in D_2O. Preference has been given to the 3D data sets, since the additional dimension helps to eliminate ambiguity in the assignments. The 2D data sets were used extensively for the aromatic regions of the spectra and other unique proton chemical shifts. So far, 772 NOE cross peaks have been assigned; 50% from the ^{15}N NOESY-HMQC, 30% from the ^{13}C NOESY-HMQC and 20% from the 2D data sets. 95% of the peaks in the ^{15}N NOESY-HMQC have been assigned; refinement of the structure will focus on assignments in other data sets.

The pattern of strong sequential NOE cross peaks (sketched in Fig. 2) gives the first indication of secondary structure. Based on the presence of strong α- to amide-proton NOE cross peaks and weak amide- to amide-proton cross peaks, residues 15–24, 27–32, 38–40, 43–54, 56–66, 92–100 and 113–120 are likely to be in extended strands, which are the building blocks for β-sheets. Based on the presence of strong amide- to amide-proton cross peaks and the absence of strong α- to amide-proton cross peaks, residues 5–10, 72–80 and 104–110 are likely to be helical.

The complete NOE data, summarized in the diagonal plot in Fig. 3, more clearly define the secondary structure of villin 14T. Antidiagonal bands identify antiparallel β-strands. Specifically, residues 17–24 form a strand antiparallel to 27–31 and 43–53. Residues 43–53 are also antiparallel to 56–66. Parallel bands at a distance from the diagonal identify parallel β-strands. Thus, residues 92–98 form a strand parallel to 56–66, and residues 37–41 pair in a parallel orientation with 114–118. These relationships define the topology of two β-sheets, a five-stranded central β-sheet and a shorter two-stranded β-sheet, given in Fig. 4. Wide bands along the diagonal are characteristic of α-helices. Based on the NOE diagonal plot in Fig. 3, residues in the ranges 71–88 and 104–110 are likely to be α-helical and are referred to as helix α2 and α3, respectively. Residues in the N-terminal part of the protein also show some suggestion of helical conformation, referred to as helix α1.

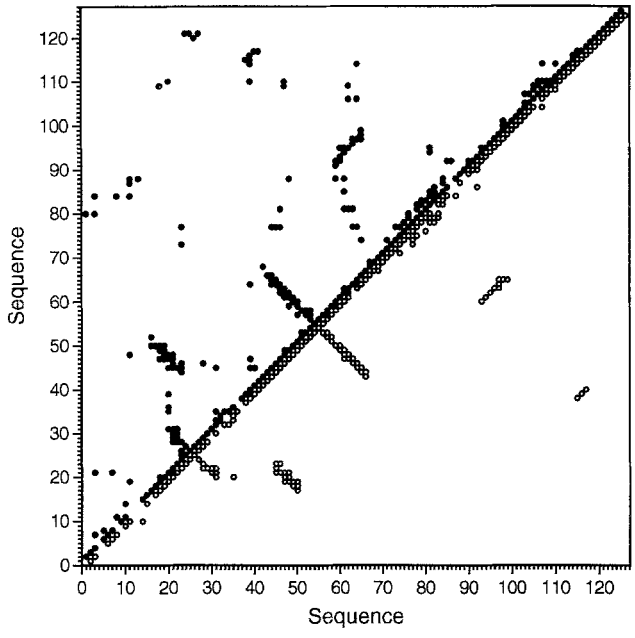

Fig. 3. Summary of assigned NOE cross peaks. This is an NOE diagonal plot, in which a symbol is plotted for each pair of residues connected by an NOE cross peak. Data above the diagonal includes cross peaks involving all protons; data below the diagonal represents cross peaks for backbone protons only. This is emphasized with filled circles for points representing cross peaks between any protons and open circles for points representing only cross peaks between backbone protons.

Secondary structure based on ^{13}C chemical shift trends

The chemical shifts themselves give an indication of the protein's secondary structure (Spera and Bax, 1991; Wishart et al., 1991; Lee et al., 1992). Specifically, the difference between the ^{13}CO chemical shift for an amino acid in the folded protein and in a 'random coil' reference state correlates with secondary structure, with positive values for α-helix and negative values for extended strands characteristic of β-sheets. The same trend is also observed for the $^{13}C^{\alpha}$ chemical shifts. Using unstructured peptides (Richarz and Wüthrich, 1978) as a reference, these differences were calculated for villin 14T and are shown in Fig. 5. A striking feature, especially for the α-carbons, is that most of the deviations are negative, supporting the classification of much of the structure as β-sheet. Groups of positive deviations are indicative of α-helices. Positive deviations for the carbonyls at positions 4–9 and the α-carbons at 6–8 are consistent with the amino-terminal helix α1. Positive deviations for carbonyls at 70–75 and 77–87 and α-carbons at 71–74 and 76–87 are consistent with helix α2. Positive deviations for carbonyls at 104 and 106–111 and α-carbons at 104–105, 107 and 111 are consistent with helix α3. Most of the other positive deviations occur at the ends or outside regular secondary structure. For example, residues 32–34 and 36 are between strands β2 and β3, 40 and 41 are at the end of strand β3, 53 and 54 are at the end of β4 and between β4 and β5, 66 and 67 are at the end of strand β5 and between β5 and helix α2, 89 and 91 are between helix α2 and strand β6, 99 and 101–103 are between strand β6 and helix α3, and residues 121, 124 and 126 are at the C-terminal end of the molecule, with undefined secondary structure.

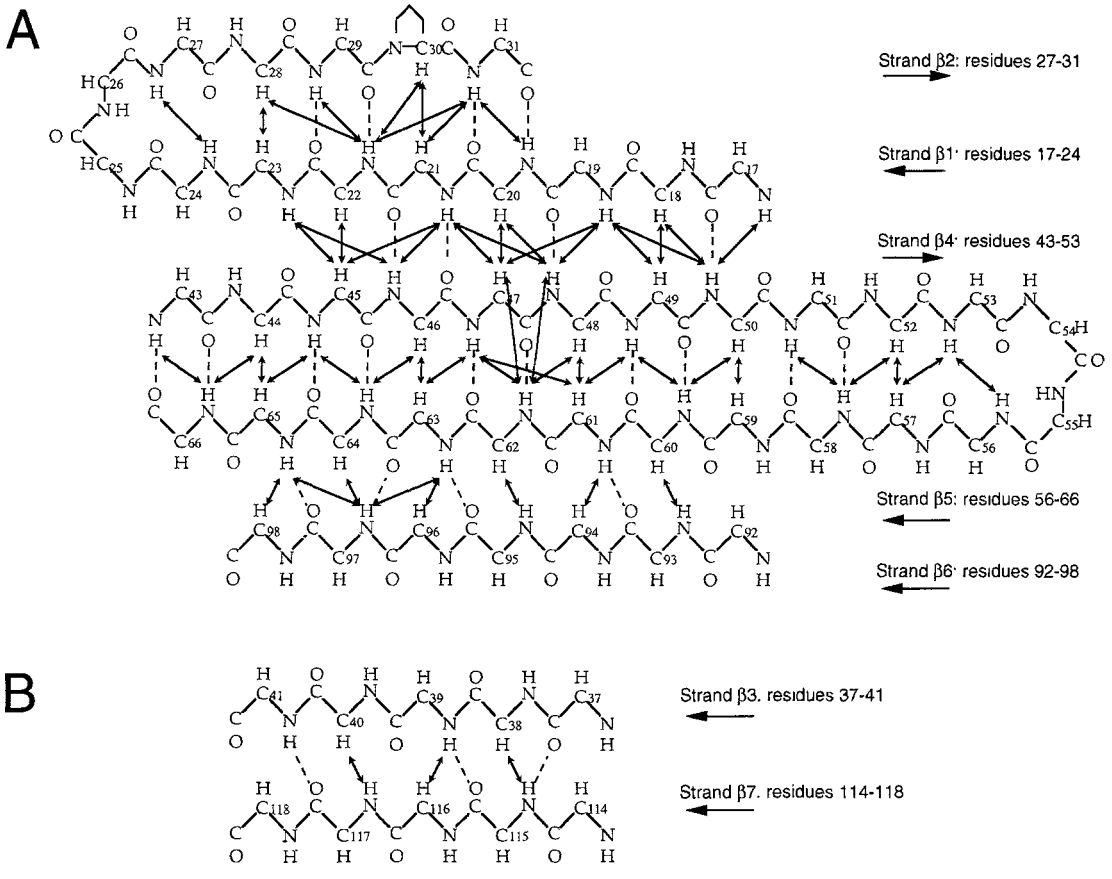

Fig. 4. β-sheets in villin 14T. (A) The main β-sheet; (B) the small parallel β-sheet. The backbone of the residues involved in the β-sheets is represented by a chemical bond drawing. Numbers on the α-carbons indicate sequence position. Double-headed arrows indicate protons connected by assigned NOE cross peaks. Dashed lines indicate hydrogen bonds supported both by the pattern of interstrand NOE cross peaks and the amide proton exchange data. The strands are labeled on the right, with arrows to indicate their relative orientations.

$^3J_{H^NH^\alpha}$ coupling constants

Vicinal coupling constants ($^3J_{H^NH^\alpha}$) between the amide- and α-protons give an indication of the backbone torsion angle ϕ. Large values of the coupling constant (> 8.0 Hz) are consistent with ϕ angles characteristic of extended strands, as in β-sheets. Small values of the coupling constant (< 5.5 Hz) are consistent with ϕ angles found in helices. $^3J_{H^NH^\alpha}$ values were measured from the peak splitting in a ^{15}N HSQC experiment with 2048 complex points in the acquisition dimension and processed with a 20°-shifted sine-squared apodization function and zero-filling to 4096 points to enhance resolution. The splitting can be seen in Fig. 1 (see for example Ser^{55} or Ile^{61}). Coupling constants were measured between contoured peak centers; since coupled peaks are in-phase and there is some overlap in the doublets, these values should be underestimates. Peaks that appeared to be unsplit or that were not sufficiently resolved to measure a splitting were arbitrarily assigned small coupling constants of 5 Hz. For 116 of the 120 assigned amide protons, values could be measured. The data are summarized in Fig. 6A. Coupling constants were also

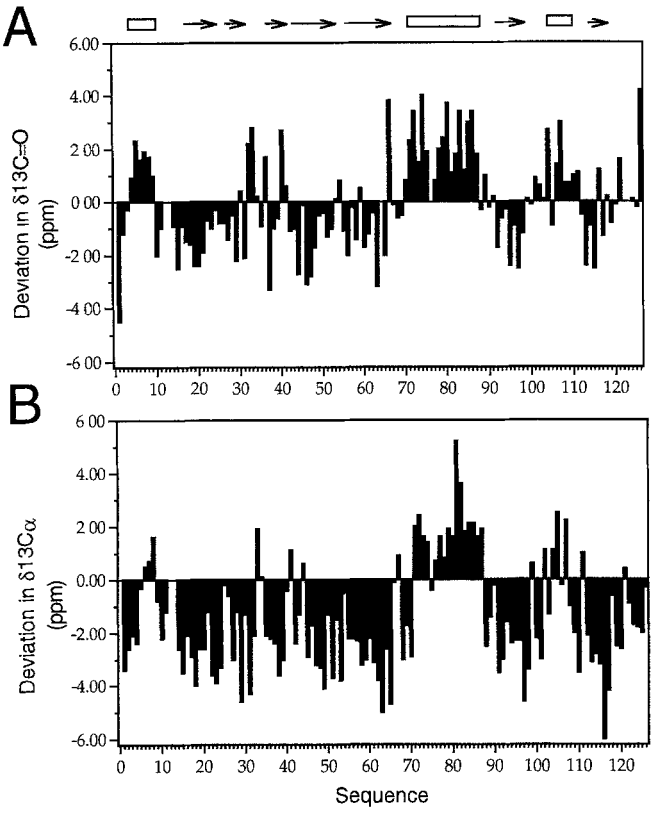

Fig. 5. Deviation from unstructured chemical shifts versus sequence for (A) carbonyl carbons and (B) α-carbons in villin 14T. Values for each amino acid type in unstructured peptides (Richarz and Wüthrich, 1978) were subtracted from the values reported in Table 1. Negative deviations are characteristic of β-sheet; positive deviations are characteristic of α-helix. Elements of secondary structure are indicated above the graphs, with open rectangles representing α-helices and arrows representing β-strands.

measured by means of the HNHA experiment, which gave values for 92 of the 120 assigned non-proline residues. Coupling constants were measured without a scale factor to account for relaxation (Vuister and Bax, 1993); therefore, these values should also be underestimates. This data is also summarized in Fig. 6A. Although both data sets should be underestimates, the values observed in both cases extend over the range expected for proteins. Comparison of the data sets suggests that for distinguishing large values of $^{3}J_{H^{N}H^{\alpha}}$ from small values, both experiments are satisfactory and their results are in accord. A more detailed comparison shows that in some cases, the results do not agree quantitatively. Most of this disagreement is due to overlap of the diagonal peaks in the HNHA spectrum. At the resolution of our data set, some diagonal peaks overlap in either the ^{15}N or the indirect ^{1}H dimension, causing errors in the volume measurements of these peaks and thus errors in the calculation of $^{3}J_{H^{N}H^{\alpha}}$. Some of the disagreement is probably also due to overlap in the multiplets observed in the ^{15}N HSQC spectrum.

The vicinal $^{3}J_{H^{N}H^{\alpha}}$ coupling constants suggest that residues 71–86 and 102–109 form helices. Residues 3–6 also show small coupling constants, characteristic of helices. Regions that corre-

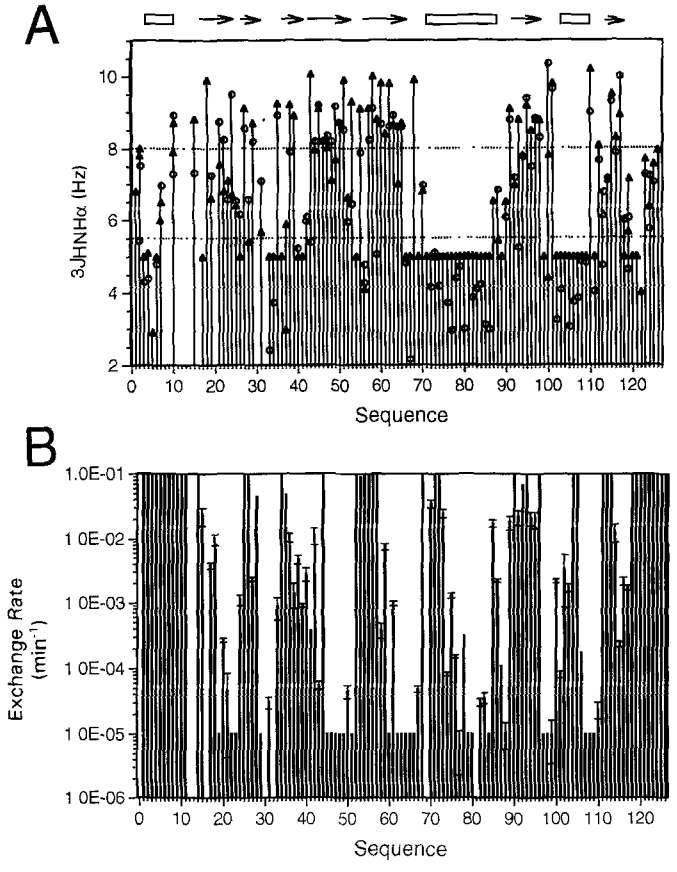

Fig. 6. (A) Summary of $^{3}J_{H^{N}H^{\alpha}}$ coupling constants for villin 14T. Coupling constants derived from the higher resolution ^{15}N HSQC are represented by triangles; values measured in the HNHA experiment are represented by circles. For residues with two sets of cross peaks, coupling constants for both peaks are included wherever they could be measured. For glycine residues, coupling constants to both α-protons are included wherever they could be measured. (B) Summary of amide proton exchange rates in D_2O at pH 4.15. Bars represent the exchange rates; error estimates are added to the bars wherever available. For amide protons which exchange so rapidly that they were not observed in D_2O, the exchange rate was plotted as 1.0×10^{-1} per min. For amide protons that did not exchange, even after one week in D_2O, the exchange rate was plotted as 1.0×10^{-5} per min. For very fast and very slow exchange, no error estimates were calculated. Elements of secondary structure are indicated above the graphs, with open rectangles representing α-helices and arrows representing β-strands.

spond to extended strands, based on $^{3}J_{H^{N}H^{\alpha}}$ values, include residues 43–53, 57–65, 91–98 and 115–117.

Exchange rates for backbone amide protons in D_2O

Exchange of amide protons in D_2O was monitored in a series of ^{15}N HSQC experiments. Slow exchange implies the presence of a hydrogen bond. Therefore, the pattern of slowly exchanging amides can be used to identify patterns of hydrogen bonds corresponding to regular secondary structure. The exchange rates for amide protons in villin 14T are summarized in Fig. 6B. Values could be measured for 116 of the 120 assigned amide protons; for two pairs of peaks, overlap prevented unambiguous interpretation. Amide protons in residues 17–24 (except Ile^{18}, which

overlaps with Asn[68] and could not be resolved) have reduced exchange rates, consistent with identification of these residues as an internal strand of the main β-sheet. Amide protons in residues 27–31 display reduced exchange rates, with faster exchange for Met[28] (Pro[30] has no amide proton) and slower exchange for Glu[27], Val[29] and Val[31]. This pattern is consistent with identification of these residues as an edge strand of the main β-sheet, with one side somewhat solvent exposed and the other hydrogen bonded into the sheet. Residues 37–41 also display some alternation in the context of reduced exchange rates, consistent with their position at one edge of the smaller β-sheet. Residues 45–51 and 58–67 show a continuous pattern of slowly exchanging amides, consistent with their identification as internal strands of the main β-sheet. Residues 92–98, which were identified as a parallel strand at the edge of the main β-sheet, do not show the characteristic pattern of alternating fast and slow exchange. Since the geometry for parallel strands is slightly different from that for antiparallel strands, residues 92–98 may hydrogen bond less well to their neighboring strand which accommodates antiparallel interactions with the strand on the other side. Alternatively, residues 92–98 may not show slowly exchanging amides because the strand is on the edge of the sheet and is solvent accessible. Residues 114–117 again show alternating rates in the context of reduced exchange; this is consistent with their role as the other edge of the smaller β-sheet. The N-terminal helix, suggested by NOE and $^3J_{H^N H^\alpha}$ data, is not supported by the exchange data. Slow exchange in residues 74–88 is consistent with helix α2 from 71–88. The more rapid exchange for residues 85 and 86 implies an irregularity in the helix at that point. Slow exchange in residues 106–110 is consistent with helix α3 from 104–110.

pH and calcium titrations

Amide chemical shift assignments were transferred to more neutral pH values and then to higher calcium concentrations on the basis of a series of ^{15}N HSQC spectra. The pH and calcium concentrations were increased in small steps, so that assignments could be transferred by assuming that the changes in chemical shifts between two adjacent spectra in the series were in general small. Ambiguities result when two or more peaks overlap. In most cases these ambiguities can be resolved by considering the direction and size of the movement of the peaks in previous spectra. Four pairs of peaks (Gly[17] and Gly[54], Ile[18] and Asn[68], Ser[69] and Thr[81], Gly[89] and Gly[120]) overlap in the initially assigned spectrum at pH 4.10, no calcium. These peaks have tentatively been assigned based on the movements of nearby peaks in the sequence. However, since these peaks do not move very much during the titrations, reversal of these assignments would not affect the conclusions.

The changes in the chemical shift assignments from pH 4.10 to 6.91 are summarized in Fig. 7. For most residues, the changes are small, with 70% of the amide proton chemical shifts moving less than 0.10 ppm and 75% of the amide nitrogen chemical shifts moving less than 0.5 ppm. Small changes in chemical shift for most of the sequence suggest that the overall structure of the protein does not change very much on going to neutral pH. Large changes in chemical shift are observed for some residues. Amide protons of Cys[44], Ser[70], Ala[92] and Val[121] move by more than 0.50 ppm; amide nitrogens of Ser[90], Ala[92], His[95] and Val[121] move by over 2.0 ppm. Cys[44] is near the end of strand β4, Ser[70] is between strand β5 and helix α2, Ser[90] is between helix α2 and strand β6, Ala[92] and His[95] are in strand β6 (at the edge of the sheet), and Val[121] is in the carboxyl-terminal part of the chain, with no identified secondary structure. Therefore, most of the chemical shifts that move are associated with amides near the surface of the molecule and outside elements of regular

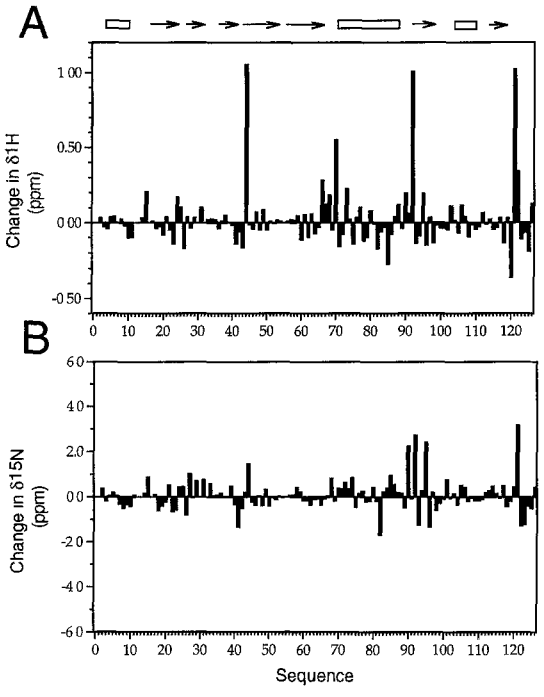

Fig. 7. Changes in chemical shift observed during the pH titration for (A) the amide protons and (B) the amide nitrogens. Each bar represents the difference between the assigned chemical shift at pH 6.91 and 4.10 for the amide in the corresponding sequence position. Elements of secondary structure are indicated above the graphs, with open rectangles representing α-helices and arrows representing β-strands.

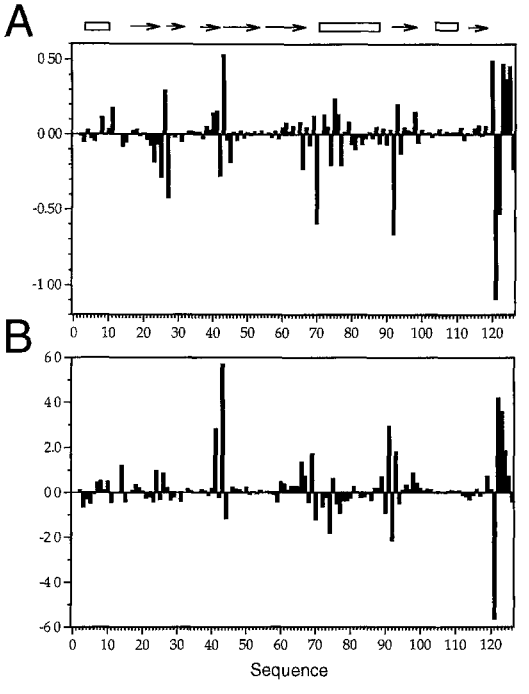

Fig. 8. Changes in chemical shift observed during the calcium titration for (A) the amide protons and (B) the amide nitrogens. Each bar represents the difference between the assigned chemical shift in 50 mM Ca^{2+} and no calcium for the amide in the corresponding sequence position. Elements of secondary structure are indicated above the graphs, with open rectangles representing α-helices and arrows representing β-strands.

secondary structure. This observation supports the assertion that the overall structure of the protein does not change on going to higher pH.

The changes in the amide chemical shifts from 0.0 to 50.0 mM calcium are summarized in Fig. 8. Again, changes for most residues are small, with about 74% of the amide protons moving less than 0.10 ppm and 75% of the amide nitrogens moving less than 0.5 ppm. Again, this suggests that 14T did not experience significant refolding as calcium was added. The largest changes, above 0.50 ppm in proton and above 2.0 ppm in nitrogen chemical shifts, occur for Asp^{43}, Ser^{70}, Val^{91}, Ala^{92}, Val^{121} and Ala^{122}. These residues are primarily at the edge or outside elements of secondary structure and near the surface of the domain.

DISCUSSION

Secondary structure in villin 14T

From the NOE, $^3J_{H^N H^\alpha}$ and hydrogen exchange data presented above, a consistent picture of the secondary structure of villin 14T emerges. The main feature of the domain is a five-stranded

β-sheet, given in detail in Fig. 4A. The topology is β2, β1, β4, β5 and β6. The strands are antiparallel to each other, except for strand β6, which is parallel to strand β5. A second, smaller β-sheet is formed by strands β3 and β7, shown in Fig. 4B. These strands are parallel to each other.

There are three helices in villin 14T. Helix α1 is in the N-terminal part of the protein, roughly from residues 1–11. Helices α2 and α3 include residues 71–88 and 104–110, respectively. Evidence for helices α2 and α3 is clear in the patterns of strong $d_{NN}(i,i+1)$ NOEs, the medium-range NOEs, the $^3J_{H^NH^\alpha}$ coupling constants and the amide proton exchange rates over most of their lengths. The deviations of the ^{13}C chemical shifts from random coil values also support the presence of these helices. The exact boundaries of the helices are not very well defined; the ranges quoted are based on continuous stretches of (i,i+3) and (i,i+4) NOE cross peaks.

The existence of helix α1 is supported by strong $d_{NN}(i,i+1)$ NOEs for residues 6, 7 and 10, small $^3J_{H^NH^\alpha}$ coupling constants for residues 3–6, and some additional NOEs for residues 3, 5, 7, 8 and 11. These NOEs include one (i,i+3) cross peak from Lys^5 to Thr^8 and another one from Thr^8 to Leu^{11}, as well as two (i,i+4) cross peaks between Leu^3 and Val^7. The existence of this helix is also supported by the ^{13}C chemical shift trends. Positive deviations are observed for the α-carbon chemical shifts in residues 6–8 and for the carbonyl chemical shifts in residues 4–9. The helix is not apparent in the hydrogen exchange data. However, considering the short extent of the helix, and the fact that the first residues of a helix are not involved in hydrogen bonds, this is not very surprising. The boundaries of helix α1 are difficult to determine, because there are relatively few medium-range NOE cross peaks assigned in this region. Interpretation of the NOE data is complicated by the lack of assignments for Asp^{12} and Lys^{13}, the doubling of peaks for residues 1–5, 7, 8, and 10–11, and the local shortage of readily identifiable, unique chemical shifts. However, additional support for an α-helix within the first 11 residues of villin 14T comes from the pattern of NOEs to helix α2. Val^1, Leu^3, Thr^8 and Leu^{11} side chains show NOE cross peaks to Tyr^{80}, Met^{84}, Tyr^{87} and Leu^{88}. The spacing of the residues which pack into helix α2 implies a helical conformation in residues 1–11. Relatively large $^3J_{H^NH^\alpha}$ coupling constants for Glu^2 and Lys^{10} suggest that the actual helix may be limited to residues 3–9. The highly homologous protein gelsolin (McLaughlin et al., 1993) also has an N-terminal helix, comprising the residues corresponding to 6–10 in villin 14T. As more NOE cross peaks are assigned and the structure is refined, the boundaries of helix α1 will probably become clearer.

Tertiary structure of villin 14T

From the NOE diagonal plot, we begin to get an idea of how the elements of secondary structure pack. The structure of villin 14T has been calculated by the distance geometry algorithm (Havel, 1991) and is presented in detail elsewhere (Markus et al., 1994). The coordinates have been deposited with the Brookhaven Protein Data Bank as entry 1VIL. A ribbon diagram, based on that structure, is presented in Fig. 9 to summarize the secondary structure and demonstrate how the elements pack. The five-stranded β-sheet forms the center of the structure. Helices α1 and α2 are parallel to each other and to the strands of the main β-sheet. They cover one face of the sheet. Helix α3 covers part of the opposite face of the main β-sheet, and its axis is nearly perpendicular to the strands of the β-sheet. The small parallel sheet is on the same side of the main β-sheet as helix α3. While strand β3 and β7 are roughly parallel to the strands in the main β-sheet, the plane of the smaller β-sheet is at an angle to the plane of the main β-sheet.

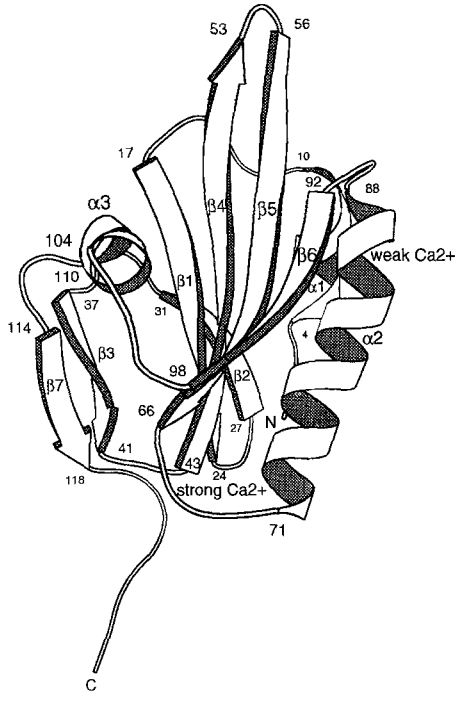

Fig. 9. Ribbon diagram of villin 14T, identifying elements of secondary structure. 'N' and 'C' denote the amino-terminal and carboxyl-terminal ends of the peptide chain. Extended strands involved in β-sheet are labeled β1 through β7, in order by chemical sequence. α-helices are labeled α1 through α3. The two regions implicated in Ca^{2+} binding are also labeled. Numbers give the sequence positions of the end points of the secondary structure elements. The diagram was generated with MOLSCRIPT (Kraulis, 1991).

Calcium binding by 14T

Comparison of Figs. 7 and 8 reveals that the peaks which move the most in the pH titration tend to move back in the calcium titration. This suggests that the local chemical environments for these amides are similar at low pH (4.10) and at neutral pH (6.91), 50 mM calcium. In the pH range 4.10–6.91, the main changes in the functional groups of proteins are deprotonation of the acidic side chains of aspartate and glutamate to form carboxylate anions and deprotonation of the cationic histidine side chains to form neutral species. As the most likely ligands for calcium cations are carbonyl and carboxyl oxygens (Strynadka and James, 1991), this suggests an explanation for the observed changes in amide chemical shifts. As the acidic side chains become deprotonated, they partially offset their negative charges by hydrogen bonding to nearby amides. As calcium is added, calcium ligation competes with hydrogen bond formation, until the hydrogen bonds are disrupted. In this sense, the structure at low pH is more similar to the Ca^{2+}-bound form at neutral pH.

To locate the putative calcium-binding sites, the amides with the largest chemical shift changes during the calcium titration were located on the structure. Asp^{43} is the first residue of strand β4, while Ser^{70} is positioned between neighboring strand β5 and helix α2. Val^{91} and Ala^{92} are at the opposite end of helix α2, leading into strand β6. Val^{121} and Ala^{122} have NOE cross peaks to Glu^{24}

and Glu^{27} in the turn between strands β1 and β2, adjacent to strand β4 in the central β-sheet. Asp^{43}, Ser^{70}, Val^{121} and Ala^{122} are relatively close together, at the 'bottom' of the central β-sheet and helix α2 in Fig. 9. Val^{91} and Ala^{92} are far from this site, near the 'top' of helix α2 and the central β-sheet in Fig. 9. This suggests that there are two calcium-binding sites. Calcium-binding curves for individual amides reveal a smaller dissociation constant for the amides near the bottom of the sheet compared to the amides at the top of the helix, confirming the presence of two sites. Two sites for calcium have also been observed in the gelsolin segment 1–actin complex (McLaughlin et al., 1993). The calcium-binding site at the bottom of the sheet corresponds to an intramolecular site in gelsolin segment 1, while the site at the top of the helix corresponds to an intermolecular site formed with actin. Dissociation constants and likely carboxylate ligands have been presented together with a more detailed comparison with gelsolin segment 1 (Markus et al., 1994).

CONCLUSIONS

The assignments for villin 14T have provided the basis for detailed studies of the structure in solution. Further, the assignments permit the interpretation of chemical shifts as atomic-resolution probes into the structure. The chemical shifts for the amide nitrogens and protons have been used as probes under different pH and calcium conditions. While the overall fold of the domain apparently remains the same under these conditions, significant changes occur in two general regions on the surface of the protein. These regions correspond to two binding sites for calcium cations.

ACKNOWLEDGEMENTS

This work was supported by NIH Grants GM 38608 (G.W.) and DK 35306 (P.M.). Computer facilities used for structure calculations were funded in part by the W.M. Keck Foundation. We thank Michael Way for the plasmid used in the expression of villin 14T and Lawrence McIntosh for acquiring the initial spectra and stimulating interest in the project. We also thank Andrzej Krezel for assistance with computers, and N.R. Nirmala, K. Chandrasekhar and Peter Schmieder for assistance with the spectroscopy.

REFERENCES

Archer, S.J., Ikura, M., Torchia, D.A. and Bax, A. (1991) *J. Magn. Reson.*, **95**, 636–641.

Archer, S.J., Vinson, V.K., Pollard, T.D. and Torchia, D.A. (1993) *Biochemistry*, **32**, 6680–6687.

Barna, J.C.J., Laue, E.D., Mayger, M.R., Skilling, J. and Worall, S.J.P. (1987) *J. Magn. Reson.*, **73**, 69–77.

Bax, A. and Ikura, M. (1991) *J. Biomol. NMR*, **1**, 99–104.

Bazari, W.L., Matsudaira, P., Wallek, M., Smeal, T., Jakes, R. and Ahmed, Y. (1988) *Proc. Natl. Acad. Sci. USA*, **85**, 4986–4990.

Bodenhausen, G. and Ruben, D.J. (1980) *Chem. Phys. Lett.*, **69**, 517–552.

Braunschweiler, L. and Ernst, R.R. (1983) *J. Magn. Reson.*, **53**, 521–528.

Brown, S.C., Weber, P.L. and Mueller, L. (1988) *J. Magn. Reson.*, **77**, 166–169.

de Arruda, M.V., Bazari, H., Wallek, M. and Matsudaira, P. (1992) *J. Biol. Chem.*, **267**, 13079–13085.

Forman-Kay, J.D., Clore, G.M., Driscoll, P.C., Wingfield, P., Richards, F.M. and Gronenborn, A.M. (1989) *Biochemistry*, **28**, 7088–7097.

Grzesiek, S. and Bax, A. (1992) *J. Magn. Reson.*, **96**, 432–440.
Havel, T.F. (1991) *Prog. Biophys. Mol. Biol.*, **56**, 43–78.
Janmey, P.A. and Matsudaira, P.T. (1988) *J. Biol. Chem.*, **263**, 16738–16743.
Kay, L.E., Ikura, M., Tschudin, R. and Bax, A. (1990) *J. Magn. Reson.*, **89**, 496–514.
Kay, L.E., Xu, G., Singer, A.U., Muhandiram, D.R. and Forman-Kay, J.D. (1993) *J. Magn. Reson. Ser. B*, **101**, 333–337.
Kraulis, P. (1991) *J. Appl. Crystallogr.*, **24**, 946–950.
Lee, M.S., Palmer, A.G. and Wright, P.E. (1992) *J. Biomol. NMR*, **2**, 307–322.
Majumdar, A., Wang, H., Morshauser, R.C. and Zuiderweg, E.R.P. (1993) *J. Biomol. NMR*, **3**, 387–397.
Marion, D., Driscoll, P.C., Kay, L.E., Wingfield, P.T., Bax, A., Gronenborn, A.M and Clore, G.M. (1989a) *Biochemistry*, **28**, 6150–6156.
Marion, D., Kay, L.E., Sparks, S.W., Torchia, D.A. and Bax, A. (1989b) *J. Am. Chem. Soc.*, **111**, 1515–1517.
Marion, D., Ikura, M. and Bax, A. (1989c) *J. Magn. Reson.*, **84**, 425–430.
Markus, M.A., Nakayama, T., Matsudaira, P. and Wagner, G. (1994) *Protein Sci.*, **3**, 70–81.
Matsudaira, P. and Janmey, P. (1988) *Cell*, **54**, 139–140.
McIntosh, L.P. and Dahlquist, F.W. (1990) *Q. Rev. Biophys.*, **23**, 1–38.
McLaughlin, P.J., Gooch, J.T., Mannherz, H.G. and Weeds, A.G. (1993) *Nature*, **364**, 685–692.
Messerle, B.A., Wider, G., Otting, G., Weber, C. and Wüthrich, K. (1989) *J. Magn. Reson.*, **85**, 608–613.
Metzler, W.J., Constantine, K.L., Friedrichs, M.S., Bell, A.J., Ernst, E.G., Lavoie, T.B. and Mueller, L. (1993) *Biochemistry*, **32**, 13818–13829.
Neri, D., Szyperski, T., Otting, G., Senn, H. and Wüthrich, K. (1989) *Biochemistry*, **28**, 7510–7516.
Olejniczak, E.T. and Eaton, H.L. (1990) *J. Magn. Reson.*, **87**, 628–632.
Piantini, U., Sørensen, O.W. and Ernst, R.R. (1982) *J. Am. Chem. Soc.*, **104**, 6800–6801.
Pope, B., Way, M. and Weeds, A.G. (1991) *FEBS Lett.*, **280**, 70–74.
Powers, R., Gronenborn, A.M., Clore, G.M. and Bax, A. (1991) *J. Magn. Reson.*, **94**, 209–213.
Richarz, R. and Wüthrich, K. (1978) *Biopolymers*, **17**, 2133–2141.
Schmieder, P., Stern, A.S., Wagner, G. and Hoch, J.C. (1994) *J. Biomol. NMR*, **4**, 483–490.
Schutt, C.E., Myslik, J.C., Rozycki, M.D., Goonesekere, N.C.W. and Lindberg, U. (1993) *Nature*, **365**, 810–816.
Senn, H., Werner, B., Messerle, B.A., Weber, C., Traber, R. and Wüthrich, K. (1989) *FEBS Lett.*, **249**, 113–118.
Sklenar, V., Piotto, M., Leppik, R. and Saudek, V. (1993) *J. Magn. Reson. Ser. A*, **102**, 241–245.
Spera, S. and Bax, A. (1991) *J. Am. Chem. Soc.*, **113**, 5490–5492.
Strynadka, N.C.J. and James, M.N.G. (1991) *Curr. Opin. Struct. Biol.*, **1**, 905–914.
Szyperski, T., Neri, D., Leiting, B., Otting, G. and Wüthrich, K. (1992) *J. Biomol. NMR*, **2**, 323–334.
Vinson, V.K., Archer, S.J., Lattman, E.E., Pollard, T.D. and Torchia, D.A. (1993) *J. Cell Biol.*, **122**, 1277–1283.
Vuister, G.W. and Bax, A. (1993) *J. Am. Chem. Soc.*, **115**, 7772–7777.
Way, M. and Weeds, A.G. (1988) *J. Mol. Biol.*, **203**, 1127–1133.
Way, M., Pope, B. and Weeds, A.G. (1992) *J. Cell Biol.*, **119**, 835–842.
Wishart, D.S., Sykes, B.D. and Richards, F.M. (1991) *J. Mol. Biol.*, **222**, 311–333.
Wüthrich, K. (1986) *NMR of Proteins and Nucleic Acids*, Wiley, New York, NY.